# Fully Analytical Approach to Calibration of Six-Port Reflectometers Using Matched Load and Unknown Loads for One-Port Measurements

Kamil Staszek

*Abstract*— In this article, the first fully analytical procedure for calibration of six-port reflectometers with a match load and unknown calibration loads, allowing for relative measurements of complex reflection coefficient, is proposed. The used loads may vary in both magnitudes and phases, with no particular requirement on their values; however, for a good performance, they should be reasonably spread over the complex plane. The proposed closed-form solution for six-port reflectometers' calibration does not require any sophisticated numerical algorithm or convergence analysis. Hence, it is significantly simpler to implement even in systems with reduced computational resources. The comparison against the previously reported numerical solution shows that the execution time is reduced by a factor of 800. The calibration is validated with the use of two six-port reflectometers with integrated power detectors over a bandwidth of 2.5–3.5 GHz. The results confirm high robustness to imperfect power measurement and very good agreement with values measured using a commercial vector network analyzer (VNA) for a large range of both magnitude and phase of the measured reflection coefficients.

*Index Terms*— Calibration, power measurement, quadric surface, reflection coefficient, reflectometer, six-port.

## I. INTRODUCTION

**M**EASUREMENT of complex scattering parameters is one of the most fundamental and frequent actions in contemporary microwave electronics. Nowadays, such measurements are realized with the use of a vector network analyzer (VNA), which is a substantial equipment in most of the microwave laboratories. Because of their complexity VNAs are bulky and expensive, which eliminates their application in low-cost and/or mobile devices. In this area, six-port reflectometers are an interesting alternative. A six-port reflectometer is composed of a six-port passive network distributing microwave signal from the source to four power detectors and devices under test (DUT) [1]. A properly designed signal distribution realized by the mentioned six-port network allows for deriving complex reflection coefficients from the power values. Six-port reflectometers do not need any frequency conversion circuits; hence, they exhibit simple circuitry, high linearity, as well as high power efficiency [2], [3].

Thanks to their advantages, six-port reflectometers found a wide area of applications, mainly in microwave sensors, where a small, reliable system is needed for complex reflection coefficient measurement. Examples can be found in permittivity measurements [4], modulators and demodulators of RF signals [5], or in radars [6], [7]. Also, since the six-port networks are fully passive, they are easily scalable with frequency, meaning that a given circuit topology can be realized for various frequency ranges. This phenomenon distinguishes six-port reflectometers from other measurement techniques, like mixer-based ones, in which the cutoff frequency of active elements constitutes a fundamental limitation. Therefore, six-port reflectometers allow for the realization of simple measurement circuitry operating in the mm-wave frequency range [8], as well as in the optical range [9], [10].

Regardless of the application, each six-port reflectometer needs to be calibrated before actual measurement. As with every practical circuit, they may exhibit magnitude and phase imbalances, as well as nonidentical sensitivity of power detectors, which lead to systematic errors arising in the measurement results. Calibration is required to suppress these errors. In general, the calibration procedures for six-port reflectometers can be divided into two major groups. The first one is constituted by methods using a set of precisely known so-called "calibration standards." Then, system constants, being the result of calibration, are derived using the known reflection coefficients of the used calibration standards and the corresponding power values. Such methods are quite common; they are based on analytical [11], [12], [13], [14] and numerical [15], [16] approaches; however, they require prior characterization of the calibration standards. Also, any deterioration of these calibration standards directly affects the calibration results.

An interesting modification of such a calibration method is reported in [17], where instead of using a set of fixed calibration standards, a multistate tuner with an adjustable reflection coefficient is applied. It is used to find values for particular power detectors that indicate zero-incident power as the first calibration stage. In this method, the resulting accuracy is, however, limited by the number of states of the used tuner and its repeatability. Hence, such a method is rather designated for laboratory environment, and it is difficult to implement in portable, low-cost devices.

The second group of calibration procedures is formed by methods that use unknown calibration standards. They are mainly based on the ellipse fitting approach, which requires

at least five unknown calibration loads, which may have arbitrary phases; however, they all have to share equal magnitude [18], [19]. In practice, such calibration standards are realized as different positions of movable short or, in six-port-based radars, by different positions of a target illuminated by radar. In both cases providing a number of calibration standards having identical magnitudes becomes particularly difficult with increasing frequency of operation due to insertion losses or free-space attenuation.

The above limitation has been recently overcome in [20], where for the first time, a procedure for calibrating a six-port reflectometer with the use of a matched load and loads having unknown reflection coefficients is reported. In this procedure, the calibration loads can exhibit reflection coefficients having arbitrary and not equal both magnitudes and phases. Although the requirements on calibration loads are now relaxed, the trade-off is the high complexity of the algorithm, and thus, large computational effort since the procedure requires several numerical multidimensional optimizations. Hence, also initial conditions and algorithm convergence must be taken into consideration. All this significantly extends computational time and makes the method suitable only for measurement systems with large computing resources.

In contrast to the method presented in [20], this article presents the first fully analytical procedure for the calibration of six-port reflectometers using matched load and unknown calibration loads. It allows for relative measurements, such as phase shifts and/or magnitude ratios, which are of high importance in modern electronics. As in [20], the reflection coefficients of the used loads can vary in both magnitude and phase, which greatly simplifies the selection or realization of the needed calibration kit. The proposed procedure does not require any numerical optimization algorithms, simultaneously exhibiting high robustness to imperfect power measurement realized with practical power detectors. Also, no convergence analysis is needed, and the overall execution time is incomparably lower than in the case of the numerical method reported in [20].

The proposed calibration is verified experimentally in two six-port reflectometers operating over a wide frequency range from 2.5 to 3.5 GHz for a set of one-ports exhibiting a large range of reflection coefficients' magnitudes and phases. For both reflectometers, the reflection coefficients are measured using the proposed calibration and a reference one, in which the same set of calibration loads is measured using VNA and then used as known values. It is shown that in both cases, the measured results are in very good agreement, although the proposed calibration uses the loads as unknown values. Moreover, the results are comparable to the ones obtained with the aid of a commercial VNA, which confirms the correctness of the proposed procedure.

## II. THEORETICAL MODEL OF A SIX-PORT REFLECTOMETER

A six-port reflectometer is schematically shown in Fig. 1. It consists of a six-port passive power distribution network, four power detectors, a signal source, and DUT exhibiting reflection coefficient $\Gamma$. The mentioned six-port network,
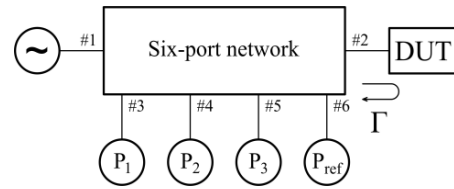


Fig. 1. Block diagram of a six-port reflectometer.

being a key element in the system, distributes excitation signal from the source to DUT and all the power detectors $P_1$–$P_3$ and $P_{ref}$; further, the signal reflected from DUT at port #2 is distributed backward to power detectors $P_1$–$P_3$ only. The value of power $P_{ref}$ is, therefore, independent of the measured reflection coefficient $\Gamma$ and can be used to monitor the signal source's power level. Also, the $P_{ref}$ value can be used to normalize the power readings $P_1$–$P_3$. Then, the relation between the measured reflection coefficient $\Gamma$ and the power readings equals [1]

$$p_i = \frac{P_i}{P_{ref}} = q_i \left| 1 + A_i \Gamma \right|^2 \qquad (1)$$

where $q_i$ and $A_i$ ($i = 1, 2, 3$) are system constants that have to be found in the calibration procedure. It is seen in (1), that power normalization using $P_{ref}$ value allows for taking reflection coefficient measurements with different power levels from the signal source since the system constants do not vary with the power.

The model given by (1) can simply be rearranged to another form, which has a well-known geometrical interpretation. By substituting

$$C_i = -\frac{1}{A_i} \qquad (2)$$

$$u_i = q_i \left| A_i \right|^2 \qquad (3)$$

equation (1) becomes

$$p_i = \frac{P_i}{P_{ref}} = u_i \left| C_i - \Gamma \right|^2. \qquad (4)$$

Analyzing (4) it can be noticed that complex values $C_i$ constitute circle centers having radii $r_i$ equal to

$$r_i = \sqrt{\frac{p_i}{u_i}}. \qquad (5)$$

Simultaneously, a point on a complex plane in which these three circles intersect is the measured reflection coefficient $\Gamma$, as illustrated in Fig. 2. This geometric interpretation has been used to develop the proposed calibration procedure presented in Section III.

## III. PROPOSED SIX-PORT CALIBRATION PROCEDURE

In this section, the proposed fully analytical calibration procedure for six-port reflectometers is presented. It starts with mapping power values' triples interpreted as 3-D-vectors onto a quadric surface representing all possible values of the complex reflection coefficient $\Gamma$; further, this surface, namely paraboloid, is used to find three points, for which one of three power values is equal to zero. Both these steps are realized with unknown loads having arbitrary and different magnitudes
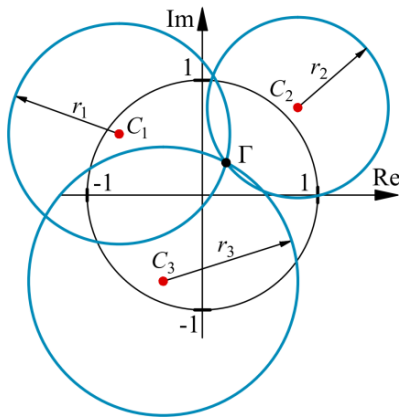
Fig. 2. Geometric model of reflection coefficient measurement with the use of a six-port reflectometer.

and phase of reflection coefficients, which eliminates the need for precise fabrication of calibration standards and their accurate characterization. In the next step, one of the calibration loads is selected as a reference value ($\Gamma = 1$), and a matched load is used to determine the center point in the mentioned quadric surface. Having power values corresponding to these two reflection coefficients and three characteristic points of the surface defined above, the scaling factors $u_i$ and circle centers $C_i$ are calculated. In the final step, the procedure is repeated to use each of the calibration loads as the reference value, and the resulting circle centers $C_i$ and scaling factors $u_i$ are averaged using weighting factors. These can easily be recalculated to $q_i$ and $A_i$ constants in (1), completing the entire procedure. As the proposed method is composed of several major stages, this section is divided into corresponding subsections presenting particular calculation steps.

### A. Quadric Surface

The relation between power readings $p_i$ and the measured reflection coefficient $\Gamma$ given by (1) or (4) shows that a three-element set of power values corresponds to certain 2-D values $\Gamma$. Hence, by generating a large set of different values $\Gamma$, a corresponding set of points forming a quadric surface in 3-D space is obtained. As reported in [21], this surface is an elliptic paraboloid, and its shape in 3-D space is determined by nine real parameters, here denoted as $a_i$, $b_i$, and $c_i$. For convenience, these parameters can be arranged in the form of the following vector:

$$\mathbf{X} = \begin{bmatrix} a_1 & a_2 & a_3 & b_1 & b_2 & b_3 & c_1 & c_2 & c_3 \end{bmatrix}^T \quad (6)$$

for which

$$\mathbf{PX} = \mathbf{1} \quad (7)$$

where $\mathbf{P}$ is a vector composed of power values $p_1$–$p_3$ obtained for a single reflection coefficient $\Gamma$

$$\mathbf{P} = \begin{bmatrix} p_1^2 & p_2^2 & p_3^2 & 2p_2p_3 & 2p_1p_3 & 2p_1p_2 & 2p_1 & 2p_2 & 2p_3 \end{bmatrix}. \quad (8)$$

Since there are nine parameters of the paraboloid (6) at least nine different reflection coefficients, or simply $N$ ($N \geq 9$) reflection coefficients $\Gamma_1$–$\Gamma_N$ have to be used to obtain $N$

rows $\mathbf{P}_n$ ($n = 1, \ldots, N$) given by (8). Then, the parameter $\mathbf{X}$ can be found by solving

$$\mathbf{X} = \left( \mathbf{P}_N^T \cdot \mathbf{P}_N \right)^{-1} \cdot \mathbf{P}_N^T \cdot \begin{bmatrix} 1 \\ \vdots \\ 1 \end{bmatrix}_{N \times 1} \quad (9)$$

where matrix $\mathbf{P}_N$ is composed of $N$ vectors $\mathbf{P}_n$ given by (8)

$$\mathbf{P}_N = \begin{bmatrix} \mathbf{P}_1 \\ \vdots \\ \mathbf{P}_N \end{bmatrix}_{N \times 9}. \quad (10)$$

It must be underlined that solving (9) requires at least nine different reflection coefficients $\Gamma_n$. They do not need to be known, and their magnitudes and phases can be arbitrary. Because of the limited measurement uncertainty of power detectors $P_1$–$P_3$ and $P_{\text{ref}}$, it is, however, advantageous to use more than nine ($N > 9$) and reasonably distributed reflection coefficients. In such a case, (9) provides the solution in the least-squares sense.

### B. Tangential Points of Quadric Surface

The quadric surface determined above contains all possible sets of power values $\{p_1, p_2, p_3\}$ obtainable for all reflection coefficients $\Gamma$. Hence, the quadric also contains points for which the reflection coefficient $\Gamma$ equals particular circle centers $C_i$. It is seen in (4) that for $\Gamma = C_i$, the normalized power $p_i = 0$; therefore, it can be concluded that the quadric given by $\mathbf{X}$ has three points, in which it is tangential to three quarter-planes, as each power can take zero value, but not negative values of course [21]. Simultaneously, for a reasonably designed six-port reflectometer, all three points $C_i$ are different from each other; therefore, if $p_i = 0$, then the remaining power values $p_j$ and $p_k$ ($j, k = 1, 2, 3$; $i \neq j$; $i \neq k$; $j \neq k$) take nonzero values. Finding all these values is a crucial step in the proposed calibration procedure.

As reported in [17], such power values can be found by means of an iterative process using a high-precision impedance tuner. Then, a large number of measurements must be taken to find the tuner's impedance, for which $p_i = 0$. This process is, therefore, time-consuming and requires dedicated circuitry with a very large number of realizable impedances since the resolution of the tuner directly impacts calibration precision. In the proposed procedure, no additional circuitry is needed, and the discussed power values $p_j$ and $p_k$, for which $p_i = 0$, can be found fully analytically, which greatly simplifies the entire process.

For determining the three sets of power values that constitute the described tangential points, the following procedure can be proposed. Assuming that $i$ is the index of power value is equal to zero ($p_i = 0$), the remaining $p_j$ and $p_k$ values can be found by rewriting (7) in expanded form, in which $p_i = 0$. Then, it takes the following form:

$$a_j p_j^2 + a_k p_k^2 + 2b_i p_j p_k + 2c_j p_j + 2c_k p_k = 1. \quad (11)$$

As can be observed, (11) describes an ellipse in $p_j$–$p_k$ plane. The desired values can then be calculated as the center point

of such an ellipse [18]. For convenience, the results can be expressed in the form of a $\mathbf{p_{min}}$ matrix having the size of $3 \times 3$, where the $i$th column represents the mentioned set of three power values, for which the quadric surface is tangential to the given quarter-plane ($p_i = 0$)

$$\mathbf{p}_{\min} = \begin{bmatrix} 0 & p_{\min}(1,2) & p_{\min}(1,3) \\ p_{\min}(2,1) & 0 & p_{\min}(2,3) \\ p_{\min}(3,1) & p_{\min}(1,3) & 0 \end{bmatrix}. \quad (12)$$

The nonzero elements of the $\mathbf{p_{min}}$ matrix are equal

$$p_{\min}(j,i) = \frac{a_k c_j - b_i c_k}{b_i^2 - a_j a_k}. \quad (13)$$

The above algorithm provides three sets of power values $\{p_1, p_2, p_3\}$, in which the quadric specified by $\mathbf{X}$ is tangential to quarter-planes. Although this approach yields correct results for theoretical power values, it may be prone to finite uncertainty power readings obtained in practical measurement systems. In case of distinct power measurement errors, the obtainable quadric may not be tangential to the quarter-planes. This can, however, easily be verified by calculating the $\mathbf{p_{min}}$ values according to (13) and then by inserting them into (7). As a result, a quadratic equation for $p_i$ is obtained, in which one of the roots should be equal to zero in an ideal case.

If, instead, $p_i$ takes nonzero values, the proposed algorithm can be augmented by simple modification. The values of $\mathbf{p_{min}}$ given by (13) can be considered as an approximation of the additional three calibration loads, which could be used in defining parameters $\mathbf{X}$ of the quadric. Therefore, the values of $\mathbf{p_{min}}$ can be used to produce additional three rows in (10). Hence, $N + 3$ calibration loads are used in finding quadric surfaces by solving (9). This process can be repeated multiple times, as with each iteration, the resulting quadric moves closer to quarter-planes, making $\mathbf{p_{min}}$ values more accurate. In practice, however, depending on power measurement inaccuracy, three to five iterations are sufficient.

### C. Scaling Factors $u_i$

The values of power $\mathbf{p_{min}}$ found above correspond to the case in which reflection coefficient $\Gamma$ equals one of the circle centers $C_i$. Hence, using (4), the following equations can be formulated:

$$|C_i - C_j| = \sqrt{\frac{p_i}{u_i}} = \sqrt{\frac{p_j}{u_j}}. \quad (14)$$

In the next step, a reference calibration load having the reflection coefficient $\Gamma_r$ has to be selected. It will serve as a normalizing value since genuine reflection coefficients of calibration loads are unknown. As a consequence, the reflection coefficient $\Gamma_r$ is assumed to be equal to $1 + j0$, which, in turn, will uniformly scale all measured reflection coefficients by its unknown value $\Gamma_r$; thus, relative measurement of magnitudes as phase differences remain unaffected, as it is described in [20]. On that basis, the following expression can be written:

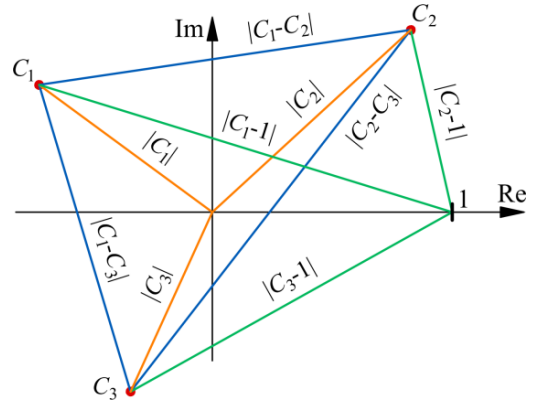$$|C_i - 1| = \sqrt{\frac{p_{ri}}{u_i}} \quad (15)$$



Fig. 3.   Geometric values used in the proposed calibration procedure.

where $p_{ri}$ is the power value measured by power detector $P_i$, when calibration load having reflection coefficient $\Gamma_r$ is connected. Additionally, a calibration load with zero reflection coefficient is needed, i.e., matched load, with the corresponding power values $p_{0i}$. For this calibration load

$$|C_i| = \sqrt{\frac{p_{0i}}{u_i}}. \quad (16)$$

It is worth mentioning that the matched load used to obtain (16) is the only load for which the reflection coefficient has to be known in the proposed calibration; moreover, it may also be used as one of the $N$ calibration loads in the determination of the quadric surface described in Section II-A.

As can be observed, (14)–(16) represent distances on a complex plane, which are schematically shown in Fig. 3. These distances will be used to calculate the scaling factors $u_i$. It can be shown that each $u_i$ can be found using (14)–(16) given for a single pair $\{i, j\}$. Such a quite straightforward procedure must be performed three times for three different pairs $\{i, j\}$; however, in the presence of noise and a distinct power detectors nonlinearity, better results are obtained when all three pairs are investigated simultaneously. It can be achieved by creating an over-determined set of equations and solving it in the least-squares sense. For this purpose, a single unknown value has to be defined

$$v = \frac{1}{u_1}. \quad (17)$$

Then, the value $v$ is the root of the equation

$$h_3 v^3 + h_2 v^2 + h_1 v + h_0 = 0 \quad (18)$$

having the maximum value among all real solutions. The coefficients $h_3$–$h_0$ are defined as follows:

$$h_3 = 2 \sum_{i \neq j} e_{ij}^2 \quad (19)$$

$$h_2 = 3 \sum_{i \neq j} e_{ij} f_{ij} \quad (20)$$

$$h_1 = 2 \sum_{i \neq j} \left( e_{ij} g_{ij} + f_{ij}^2 \right) \quad (21)$$

$$h_0 = \sum_{i \neq j} \left( f_{ij} g_{ij} \right) \quad (22)$$

where

$$e_{ij} = (\alpha_i \beta_j - \beta_i \alpha_j)(\alpha_j + \beta_i - \alpha_i - \beta_j) + \delta_{ij}(\alpha_i - \beta_i)(\beta_j - \alpha_j) \tag{23}$$

$$f_{ij} = (\alpha_i - \alpha_j)(\beta_j - \beta_i) + \delta_{ij}(\alpha_i + \beta_i + \alpha_j + \beta_j - \delta_{ij}) \tag{24}$$

$$g_{ij} = -\delta_{ij} \tag{25}$$

and

$$\alpha_i = \begin{cases} p_{0i}, & \text{for } i = 1 \\ p_{0i} \dfrac{\mathbf{p_{min}}(1, i)}{\mathbf{p_{min}}(i, 1)}, & \text{for } i \neq 1 \end{cases} \tag{26}$$

$$\beta_i = \begin{cases} p_{ri}, & \text{for } i = 1 \\ p_{ri} \dfrac{\mathbf{p_{min}}(1, i)}{\mathbf{p_{min}}(i, 1)}, & \text{for } i \neq 1 \end{cases} \tag{27}$$

$$\delta_{ij} = \begin{cases} \mathbf{p_{min}}(i, j), & \text{for } i = 1 \\ \mathbf{p_{min}}(i, j) \dfrac{\mathbf{p_{min}}(1, i)}{\mathbf{p_{min}}(i, 1)}, & \text{for } i \neq 1. \end{cases} \tag{28}$$

Once the value of $v$ is derived, the scaling factors $u_i$ can be calculated as

$$u_i = \begin{cases} \dfrac{1}{v}, & \text{for } i = 1 \\ \dfrac{1}{v} \dfrac{\mathbf{p_{min}}(i, 1)}{\mathbf{p_{min}}(1, i)}, & \text{for } i \neq 1. \end{cases} \tag{29}$$

### D. Circle Centers $C_i$—Part I

The calculated scaling factors $u_i$ allow for the determination of circle centers $C_i$. According to distances shown in Fig. 3, the points $C_i$ can be found using $p_{0i}$ and $p_{ri}$ values. These power values are used with respect to points $\Gamma = 0$ and $\Gamma = 1$, respectively. Hence, real parts of $x_i = \text{Re}[C_i]$ can be calculated directly as

$$x_i = \frac{p_{0i} - p_{ri} + u_i}{2u_i} \tag{30}$$

whereas for imaginary parts $y_i = \text{Im}[C_i]$ only their absolute values can be determined

$$y_i = \frac{\sqrt{2p_{0i}p_{ri} + 2p_{0i}u_i + 2p_{ri}u_i - p_{0i}^2 - p_{ri}^2 - u_i^2}}{2u_i}. \tag{31}$$

To choose the correct signs for imaginary parts $y_i$ an additional algorithm is needed. At this point, an assumption can be made that $y_1$ is positive; therefore, the remaining signs of $y_2$ and $y_3$ can be determined using distances

$$r_{ij} = |C_i - C_j| = \frac{1}{2}\left( \sqrt{\frac{\mathbf{p_{min}}(i, j)}{u_i}} + \sqrt{\frac{\mathbf{p_{min}}(j, i)}{u_j}} \right) \tag{32}$$

indicated by blue lines in Fig. 3. Theoretically, (32) can, however, be simplified to make the algorithm more robust to nonlinearity, and noise present in power measurements of the distances $r_{ij}$ should be calculated using (32). Now, two signs need to be determined, namely for $y_2$ and $y_3$, giving

four variations $\{++, +-, -+, --\}$. For each of them, the error $e$ can be calculated as follows:

$$e_{++} = \left| \sqrt{(x_1 - x_2)^2 + (y_1 - y_2)^2} - r_{12} \right|$$
$$+ \left| \sqrt{(x_1 - x_3)^2 + (y_1 - y_3)^2} - r_{13} \right| +$$
$$+ \left| \sqrt{(x_2 - x_3)^2 + (y_2 - y_3)^2} - r_{23} \right| \tag{33}$$

$$e_{+-} = \left| \sqrt{(x_1 - x_2)^2 + (y_1 - y_2)^2} - r_{12} \right|$$
$$+ \left| \sqrt{(x_1 - x_3)^2 + (y_1 + y_3)^2} - r_{13} \right|$$
$$+ \left| \sqrt{(x_2 - x_3)^2 + (y_2 + y_3)^2} - r_{23} \right| \tag{34}$$

$$e_{-+} = \left| \sqrt{(x_1 - x_2)^2 + (y_1 + y_2)^2} - r_{12} \right|$$
$$+ \left| \sqrt{(x_1 - x_3)^2 + (y_1 - y_3)^2} - r_{13} \right|$$
$$+ \left| \sqrt{(x_2 - x_3)^2 + (y_2 - y_3)^2} - r_{23} \right| \tag{35}$$

$$e_{--} = \left| \sqrt{(x_1 - x_2)^2 + (y_1 + y_2)^2} - r_{12} \right|$$
$$+ \left| \sqrt{(x_1 - x_3)^2 + (y_1 + y_3)^2} - r_{13} \right|$$
$$+ \left| \sqrt{(x_2 - x_3)^2 + (y_2 + y_3)^2} - r_{23} \right|. \tag{36}$$

Among these four error values, the lowest one can be selected and used to determine signs for $y_2$ and $y_3$. Finally, temporary values of circle centers $C_{i\text{temp}}$ become

$$C_{1\text{temp}} = x_1 + jy_1 \tag{37}$$

$$e_{++} = \min\{e_{++}, e_{+-}, e_{-+}, e_{--}\} \Rightarrow \begin{cases} C_{2\text{temp}} = x_2 + jy_2 \\ C_{3\text{temp}} = x_3 + jy_3 \end{cases} \tag{38}$$

$$e_{+-} = \min\{e_{++}, e_{+-}, e_{-+}, e_{--}\} \Rightarrow \begin{cases} C_{2\text{temp}} = x_2 + jy_2 \\ C_{3\text{temp}} = x_3 - jy_3 \end{cases} \tag{39}$$

$$e_{-+} = \min\{e_{++}, e_{+-}, e_{-+}, e_{--}\} \Rightarrow \begin{cases} C_{2\text{temp}} = x_2 - jy_2 \\ C_{3\text{temp}} = x_3 + jy_3 \end{cases} \tag{40}$$

$$e_{--} = \min\{e_{++}, e_{+-}, e_{-+}, e_{--}\} \Rightarrow \begin{cases} C_{2\text{temp}} = x_2 - jy_2 \\ C_{3\text{temp}} = x_3 - jy_3. \end{cases} \tag{41}$$

Note that in (37)–(41), $j$ is imaginary unit $j = \sqrt{-1}$.

### E. Circle Centers $C_i$—Part II

The above calculation of points $C_{i\text{temp}}$ is based on the assumption that $y_1 > 0$ and requires further investigation. Now, the points $C_{i\text{temp}}$ are located in correct distances with respect to each other, but due to the above assumption, it may be required

to inverse the signs for all imaginary parts $y_i$. Decision on making complex conjugate of $C_i$ may be made upon analysis of the used calibration loads $\gamma_n$, which are genuine reflection coefficients of the calibration loads $\Gamma_n$ normalized by the reflection coefficient $\Gamma_r$ of the load selected as the reference in Section II-C. To calculate the values $\gamma_n$, the coefficients $q_i$ and $A_i$ have to be obtained by rearranging (2) and (3); further, each normalized reflection coefficient $\gamma_n$ can be calculated using

$$\gamma_n = s_0 + s_1 p_{1,n} + s_2 p_{2,n} + s_3 p_{3,n} \tag{42}$$

where $p_{i,n}$ is the power value measured by the $i$th power detector for the $n$th calibration load having reflection coefficient $\Gamma_n$; furthermore

$$s_0 = \frac{q_1 q_2 q_3}{2\varepsilon}\{\tau_1(\omega_2 - \omega_3) + \tau_2(\omega_3 - \omega_1) + \tau_3(\omega_1 - \omega_2)$$
$$+ j[\tau_1(\sigma_2 - \sigma_3) + \tau_2(\sigma_3 - \sigma_1) + \tau_3(\sigma_1 - \sigma_2)]\} \tag{43}$$

$$s_1 = \frac{q_2 q_3}{2\varepsilon}[\tau_3 \omega_2 - \tau_2 \omega_3 + j(\tau_3 \sigma_2 - \tau_2 \sigma_3)] \tag{44}$$

$$s_2 = \frac{q_1 q_3}{2\varepsilon}[\tau_1 \omega_3 - \tau_3 \omega_1 + j(\tau_1 \sigma_3 - \tau_3 \sigma_1)] \tag{45}$$

$$s_3 = \frac{q_1 q_2}{2\varepsilon}[\tau_2 \omega_1 - \tau_1 \omega_2 + j(\tau_2 \sigma_1 - \tau_1 \sigma_2)] \tag{46}$$

and

$$\varepsilon = q_1 q_2 q_3[\tau_1(\sigma_2 \omega_3 - \sigma_3 \omega_2) + \tau_2(\sigma_3 \omega_1 - \sigma_1 \omega_3)$$
$$+ \tau_3(\sigma_1 \omega_2 - \sigma_2 \omega_1)] \tag{47}$$

$$\sigma_i = \text{Re}[A_i] \tag{48}$$

$$\omega_i = \text{Im}[A_i] \tag{49}$$

$$\tau_i = |A_i|^2. \tag{50}$$

Similarly, as in Section III-D in (43)–(46) $j$ is an imaginary unit $j = \sqrt{-1}$.

The calculated $N$ reflection coefficients $\gamma_n$ of the loads used in calibration may now be used to make sign corrections for imaginary parts of circle centers $y_i$. As discussed above, the proposed calibration makes use of unknown calibration loads. Although they can be unknown, they should be reasonably spread over the complex plane, i.e., they should exhibit different magnitudes and phases. In this step, only coarse information on the phase trend of their reflection coefficient is sufficient. Such information in practical measurement systems is almost always known.

Here, to address the question of imaginary parts of circle centers $y_i$ it is sufficient to state if the consecutively measured calibration loads have, on average, increasing or decreasing electrical lengths. Then, the sign of the calculated averaged phase progression $\varphi_c$ indicates whether the signs of $y_i$ are correct or they should be opposite. The phase progression $\varphi_c$ can be derived using linear regression

$$\varphi_c = \frac{2}{N^2 - N} \sum_{n=2}^{N} (n - 1)\Theta_n \tag{51}$$

where the angles $\Theta_n$ are calculated iteratively:

$$\Theta_n = \begin{cases} 0, & \text{for } n = 1 \\ \arg\left[\dfrac{\gamma_n}{\gamma_{n-1}}\right] + \Theta_{n-1}, & \text{for } n > 1. \end{cases} \tag{52}$$

Finally, the sign of $\varphi_c$ has to be compared against the sign of genuine phase progression of the used calibration loads $\varphi_g$. For example, if the calibration loads are realized as a set of transmission lines with increasing physical length (higher electrical length for higher $n$), then the genuine phase progression is negative ($\varphi_g < 0$). Hence, the final values of circle centers can be determined

$$C_i = \begin{cases} \overline{C_{i\text{temp}}}, & \text{for } \varphi_c \varphi_g < 0 \\ C_{i\text{temp}}, & \text{for } \varphi_c \varphi_g > 0 \end{cases} \tag{53}$$

where $(\overline{\phantom{x}})$ is a complex conjugate.

It is worth mentioning that such an iterative calculation of $\Theta_n$ using arguments of ratios $\gamma_n/\gamma_{n-1}$ makes the algorithm robust to phase wraps, as described in [20]. Furthermore, it must be emphasized that the above algorithm for determining phase progression $\varphi_c$ does not require calibration loads to be known, as only coarse information on the phase of their reflection coefficients in terms of increasing or decreasing values is needed. Moreover, the phases of calibration loads do not have to be arranged monotonically, as only the sign of the averaged trend is used.

### F. Weighting Factors for Increased Robustness

The above steps described in Sections II-A–II-E constitute the complete calibration procedure resulting in the determination of system constants $u_i$ and $C_i$, which can easily be recalculated to the values $q_i$ and $A_i$ seen in (1). Nevertheless, in practical measurement systems, where power values are affected by noise and nonlinearity, a deterioration is observed for small values of imaginary parts of circle centers $y_i$. As seen in Fig. 3, the calculation of $y_i$ is done using two points (0, 0) and (1, 0), and two distances $|C_i|$ and $|C_i - 1|$, which are affected by imperfect power measurement. Hence, the determination of $C_i$ becomes inaccurate for smaller $y_i$. On the other hand, the distribution of $C_i$ is normalized by the chosen reference load $\Gamma_r$. Therefore, it is beneficial to make another selection of $\Gamma_r$ and repeat the stages described in Sections II-C–II-E. Since the value $\Gamma_r$ is now changed, also the corresponding circle centers $C_i$ will be translated, and the resulting $y_i$ will be of a different, possibly higher, value. Such a procedure can be extended to consecutively use all $N$ calibration loads as the reference $\Gamma_r$. This will yield $N$ sets of $C_i$ and $u_i$, which can be averaged with weighting factors based on $y_i$ values. Since the particular calibrations are normalized to different $\Gamma_r$, they must be appropriately rescaled prior to the averaging. The values $u_i$ and $C_i$ calculated using $N$ calibrations become much more robust to power measurement uncertainty, as the deterioration for small values of $y_i$ is greatly suppressed.

To realize the algorithm proposed above, the stages described in Sections II-C–II-E should be executed $N$ times instead of one. For each execution, another calibration load with reflection coefficient $\Gamma_k$ ($k = 1, \ldots, N$) is used as the reference $\Gamma_r$ (see Section II-C), and the obtained calibration results are stored as

$$C_{i,k} = C_i \tag{54}$$

$$u_{i,k} = u_i \tag{55}$$

together with the corresponding weighting factors based on imaginary parts of the determined circle centers

$$w_{i,k} = y_i^2. \tag{56}$$

As mentioned above, for each execution, the obtained solution is normalized by the appropriate $\Gamma_r$ value. Therefore, the parameter of normalization with respect to the calibration results obtained for the first case (where $\Gamma_r$ is realized by the first calibration load) has to be stored

$$\Delta_k = \frac{\gamma_k}{\gamma_1}. \tag{57}$$

Finally, all $N$ calibrations can be equalized using factors $\Delta_k$ and averaged with weighting factors $w_{i,k}$

$$C_i = \frac{\sum_{k=1}^{N} w_{i,k} C_{i,k} \Delta_k}{\sum_{k=1}^{N} w_{i,k}} \tag{58}$$

$$u_i = \frac{\sum_{k=1}^{N} w_{i,k} u_{i,k} \Delta_k}{\sum_{k=1}^{N} w_{i,k}}. \tag{59}$$

The obtained final coefficients $C_i$ and $u_i$ can be further used to calculate $q_i$ and $A_i$ by rearranging (2) and (3). Then a complex reflection coefficient $\gamma$ (normalized by $\Gamma_1$) is equal to

$$\gamma = s_0 + s_1 p_1 + s_2 p_2 + s_3 p_3. \tag{60}$$

## IV. EXPERIMENTAL VERIFICATION

To comprehensively verify the proposed calibration procedure, it was used to calibrate two six-port reflectometers: the classic reflectometer reported in [22] and the optimized one presented in [23]. They operate over the same wide bandwidth from 2.5 to 3.5 GHz; however, they exhibit different circle centers' distribution. For the classic reflectometer, the circle centers have magnitudes equal to 1, $\sqrt{2}$, and $\sqrt{2}$, with angular differences of 135°, 90°, and 135°, respectively. On the other hand, all circle centers of the optimized reflectometer have unitary magnitude with 120° of angular separation. Both reflectometers were fed using an SMB 100A signal generator by *Rohde & Schwarz*, providing 0 dBm of power swept over the mentioned frequency range. For power measurement, four LTC5597 integrated power detectors by *Analog Devices* were used together with 16-bit analog-to-digital converters controlled by field programmable gate array (FPGA) board [24]. They offer a linear response within the range from −35 to 0 dBm at the frequencies of interest. Photographs of the developed reflectometers are shown in Fig. 4.

As described in Section II, the proposed calibration procedure requires a matched load and at least nine calibration loads, which should cover a reasonably large part of Smith's chart over the frequencies of interest; however, due to imperfect power measurement, it is advantageous to use a higher number of calibration loads. Therefore, this number was increased to 12. Each load was fabricated as a microstrip transmission line section with different electrical lengths, terminated with a short-circuited surface-mounted device (SMD) resistor having a random value from the range from 0 to 20 Ω, which corresponds to the reflection coefficients' magnitudes
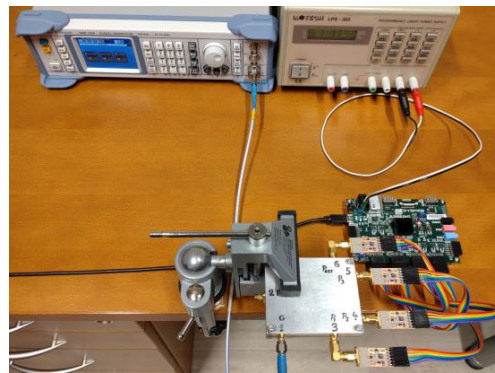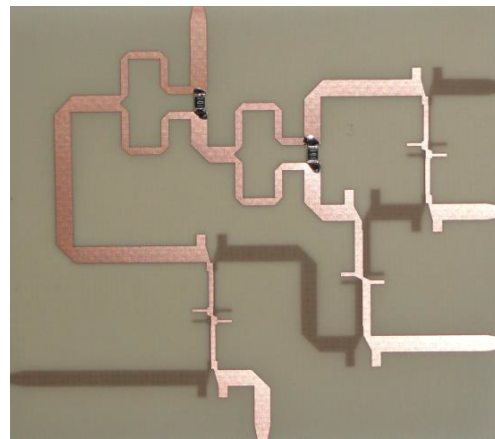


(a)
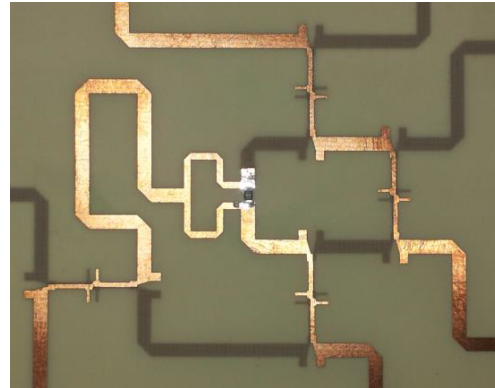


(b)
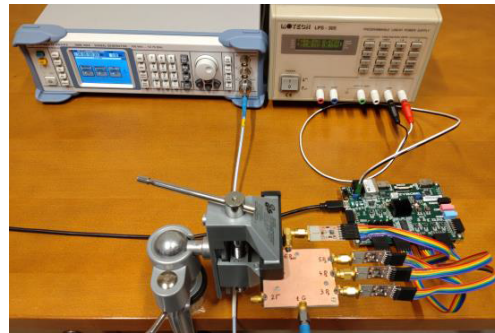


(c)



(d)

Fig. 4. Developed six-port reflectometers used to experimentally verify the proposed calibration procedure. (a) General view of the classic six-port reflectometer. (b) Layout of the classic six-port network. (c) General view of the optimized six-port reflectometer. (d) Layout of the optimized six-port network.

Fig. 5. Photograph of the match load and 12 calibration loads used in the experimental verification of the proposed calibration procedure.

TABLE I
IMPEDANCE VALUES OF THE LOADS USED IN CALIBRATION

| Cal. load | Impedance ($\Omega$) | | | |
|---|---|---|---|---|
| | 2.50 GHz | 2.83 GHz | 3.17 GHz | 3.5 GHz |
| 1 | $139+131j$ | $275+15.9j$ | $151–135j$ | $63.1–109j$ |
| 2 | $126–3.88j$ | $102–45.7j$ | $66.4–53.9j$ | $44.0–45.8j$ |
| 3 | $120–804j$ | $6.56–178j$ | $2.37–92.3j$ | $1.40–57.5j$ |
| 4 | $57.1–47.0j$ | $36.0–35.0j$ | $25.8–21.1j$ | $21.5–8.57j$ |
| 5 | $1.40–53.5j$ | $0.94–27.2j$ | $0.81–8.24j$ | $0.877+8.02j$ |
| 6 | $2.73–29.9j$ | $2.18-9.06j$ | $2.23+9.72j$ | $2.95+30.2j$ |
| 7 | $16.1–4.74j$ | $16.7+14.0j$ | $23.8+36.8j$ | $50.4+68.2j$ |
| 8 | $2.08–0.04j$ | $2.55+22.3j$ | $4.86+56.0j$ | $20.7+144j$ |
| 9 | $10.8+11.5j$ | $15.3+37.3j$ | $38.4+83.3j$ | $237+95.6j$ |
| 10 | $1.24+30.2j$ | $3.38+79.9j$ | $138+560j$ | $8.18–124j$ |
| 11 | $37.2+38.4j$ | $95.5+49.7j$ | $94.6–49.7j$ | $35.7–37.1j$ |
| 12 | $28.8+56.6j$ | $155+93.8j$ | $64.0–86.5j$ | $19.0–34.0j$ |

ranging from $\approx 0.4$ to 1. The calibration loads are shown in Fig. 5, whereas their reflection coefficients for four uniformly distributed frequencies over the range from 2.5 to 3.5 GHz are illustrated in Fig. 6; moreover, the corresponding impedances are listed in Table I. As seen, the reflection coefficients differ in both magnitudes and phases and no particular pattern in their values is observed.

The two six-port reflectometers described above were calibrated following the proposed procedure with the use of the mentioned calibration loads with no information on their reflection coefficients. It is only known that the subsequent calibration loads are of higher electrical length, hence $\varphi_g < 0$, what is inferred on the coarse view of the physical lengths of these loads seen in Fig. 5; furthermore, for both reflectometers also a reference calibration involving the same calibration loads was performed. For this purpose, however, their reflection coefficients were beforehand measured with the use of VNA and used as known values to solve (1) for $q_i$ and $A_i$ [and thus $u_i$ and $C_i$ in (4)] using the numerical procedure as described in [20]. The results of both calibrations in the form of circle centers $C_i$ for both reflectometers are shown in Fig. 7. It is seen that both calibration procedures provide similar results.

Since both reflectometers are now calibrated, they can be used to measure complex reflection coefficients. It should be emphasized that the proposed calibration allows for measuring reflection coefficients $\gamma$ normalized by the (unknown) value of the calibration load used as the first one $\Gamma_1$, marked as the dark blue filled circle in Fig. 6. As seen its magnitude
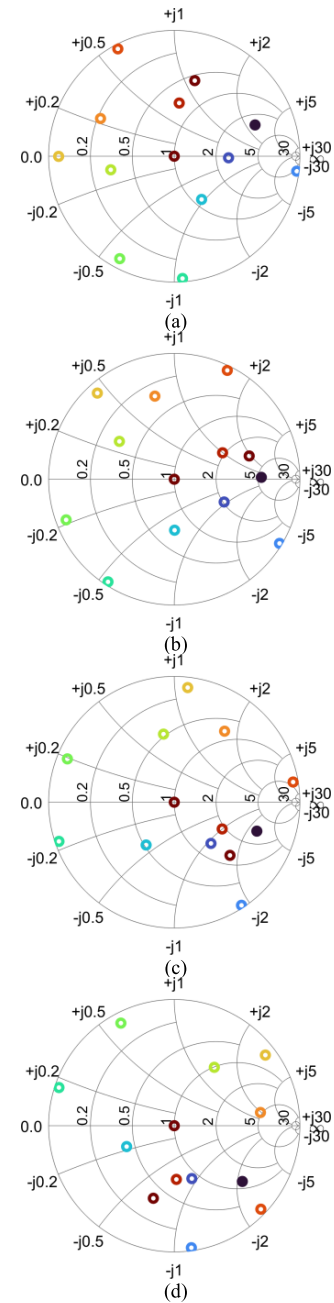


Fig. 6. Reflection coefficients of the match load and 12 calibration loads used in the experimental verification of the proposed calibration procedure for four frequencies. (a) 2.50 GHz. (b) 2.83 GHz. (c) 3.17 GHz. (d) 3.5 GHz. The reflection coefficient of the first calibration load $\Gamma_1$ is marked with a filled circle.

is lower than unity; therefore, the measured values $\gamma$ can exceed unity (or 0 dB) in magnitude. For comprehensive verification of the measurement performance, a set of six one-ports was composed of a single low-loss thru and five broadband attenuators with attenuations ranging from 1 to 10 dB. The above thru and attenuators were terminated with a sliding short having a fixed length chosen in such a way that, over the considered frequency range, their phase response varies by $\approx 360°$. As a result, the prepared one-ports exhibit reflection coefficients covering the magnitude range from $-20$ to 0 dB and all angles.

The reflection coefficients were measured using both six-port reflectometers and for both calibrations. Addition-
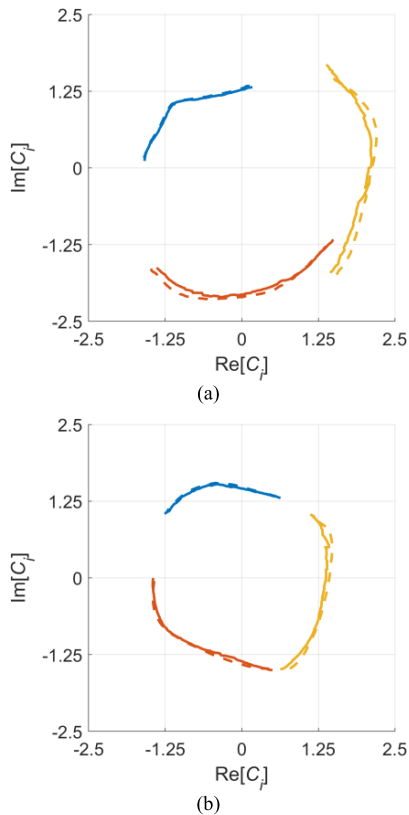
Fig. 7. Circle centers $C_i$ over the frequency range 2.5–3.5 GHz obtained in the proposed calibration (solid lines) and in the reference calibration (dashed lines) for (a) classic six-port and (b) optimized six-port.
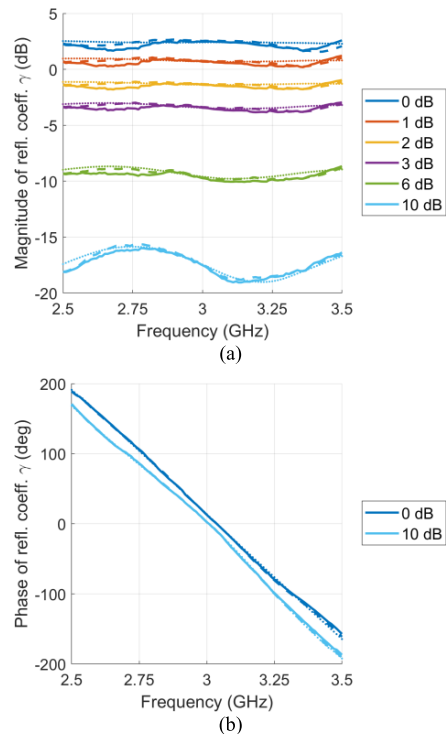


Fig. 8. Reflection coefficient of a set of one-ports composed of thru (0 dB) and five broadband attenuators having attenuation from 1 to 10 dB measured using the classic six-port reflectometer with the proposed calibration (solid lines) and with the reference calibration (dashed lines) compared against the corresponding values measured using VNA (dotted lines) over the frequency range 2.5–3.5 GHz. (a) Magnitudes. (b) Phases.

ally, the measurements were also taken with the use of a commercial VNA N5224A by *Keysight*. The values obtained for the reference calibration and the ones measured using VNA were additionally normalized by $\Gamma_1$ for better comparison against the results provided by the proposed calibration. The magnitudes and phases of the tested one-ports measured in these three ways are depicted in Fig. 8 for the classic six-port and in Fig. 9 for the optimized six-port. Because of the similar phase response of each one-ports, the phase response is only shown for the reflection coefficient having the maximum and the minimum magnitude, i.e., for 0-dB thru and for 10-dB attenuator. Furthermore, to complete the assessment of the calibration performance, error vector magnitude (EVM) was calculated for each measured one-port as

$$\text{EVM} = \left| \gamma_{\text{SP}} - \gamma_{\text{VNA}} \right| \tag{61}$$

where $\gamma_{\text{SP}}$ is the normalized reflection coefficient measured using the six-port reflectometer (classic or optimized one, with the proposed or reference calibration), and $\gamma_{\text{VNA}}$ is the corresponding value measured with the aid of VNA. The calculated values are illustrated in Fig. 10.

In the final step, the execution time of the proposed method developed in the MATLAB environment was measured. The procedure was performed on a laptop with an Intel i5 processor and 16 GB RAM. The time needed to process 101 points in frequency, for which the six-port reflectometers were calibrated, was equal to 142 ms, which corresponds to 1.4 ms for a single execution. In contrast, using the same computer, the algorithm reported in [20] requires 113 s to perform calibration

for the same number of 101 frequencies. It, therefore, equals 1.12 s for a single execution. As seen the proposed procedure reduces the execution time by 800 times.

## V. DISCUSSION

As seen in Figs. 8–10, the values measured using the proposed calibration are in good agreement with the ones obtained using the reference calibration in spite of using unknown calibration loads. It proves the correctness of the developed procedure. Although the proposed method measures values normalized by unknown reflection coefficient $\Gamma_1$, it can successfully be applied in relative measurements, such as phase shifts or magnitude ratios, which are very common in modern electronics, e.g., in microwave sensors. It is experimentally confirmed for complex values over the magnitude range exceeding 20 dB and for all possible phases.

It can also be observed that the proposed calibration provides normalized results similar to those obtained for the calibration reported in [20]. There are, however, substantial differences between these calibrations, making the presented one superior to previously reported solutions. The proposed calibration is a closed-form solution providing the results by means of fully analytical calculations. Therefore, it eliminates any need for sophisticated numerical algorithms, such as nonlinear optimizations used in [20], which usually need advanced computational resources. Also, there is no need for defining initial conditions to ensure the algorithm's convergence. Therefore, the execution time and number of calculations do not vary with input data and/or parameters of a considered
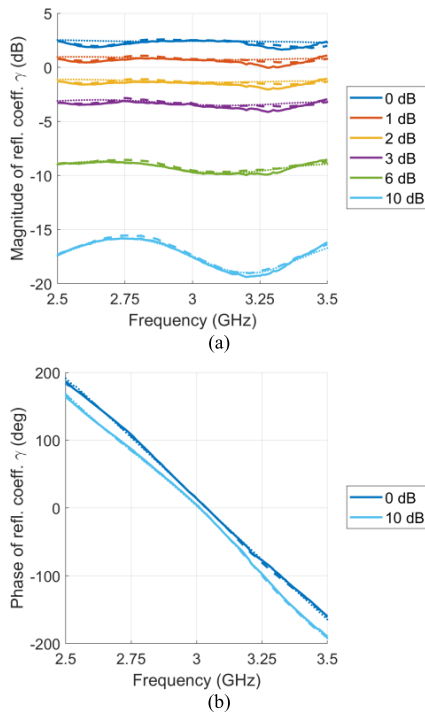
Fig. 9.   Reflection coefficient of a set of one-ports composed of thru (0 dB) and five broadband attenuators having attenuation from 1 to 10 dB measured using the optimized six-port reflectometer with the proposed calibration (solid lines) and with the reference calibration (dashed lines) compared against the corresponding values measured using VNA (dotted lines) over the frequency range 2.5–3.5 GHz. (a) Magnitudes. (b) Phases.
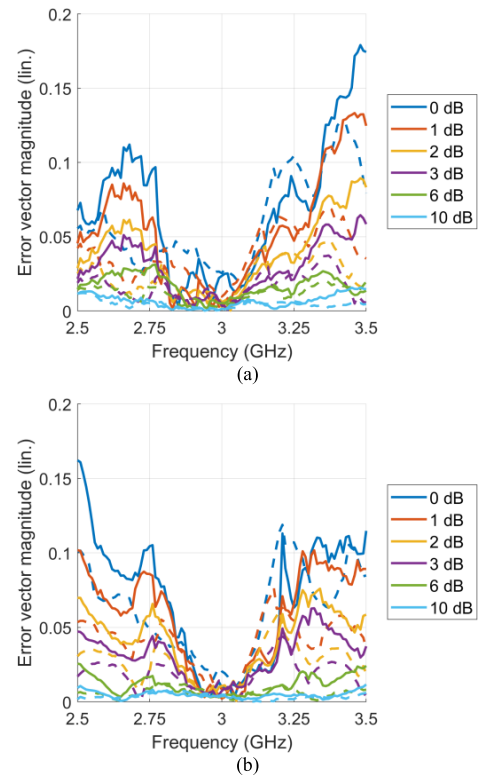


Fig. 10.   EVMs calculated for (a) classic and (b) optimized six-port reflectometers with the proposed (solid lines) and reference (dashed lines) calibration over the frequency range 2.5–3.5 GHz.

six-port reflectometer. This results in a significantly shorter time of execution and easier implementation, allowing for application in mobile devices featuring limited computational resources.

Last, a discrepancy between the measurement results obtained for both calibration procedures with respect to the values obtained using VNA needs to be addressed. As given in Section II, both the proposed calibration and the reference one are based on the model (1); thus, the ideal impedance match of the six-port network's measurement port ($s_{22} = 0$) and ideal isolation between the measurement port and the port with a reference power meter ($s_{62} = 0$) are assumed. This is, however, only an approximation since a practical six-port network exhibits small yet nonzero magnitudes of $s_{22}$ and $s_{62}$. Therefore, the model given by (1) is somehow simplified. To make it complete, it should be augmented by an $A_0$ factor corresponding to nonzero parameters $s_{22}$ and $s_{62}$ to the following form:

$$p_i = \frac{P_i}{P_{\text{ref}}} = q_i \left| \frac{1 + A_i \Gamma}{1 + A_0 \Gamma} \right|^2. \tag{62}$$

Although the model given by (62) can be solved using a procedure using known calibration loads, e.g., [15], there is no known method for solving (62) with unknown calibration loads. Simultaneously, using (1) instead of (62) for a reasonably well-designed and fabricated six-port reflectometer introduces a small systematic error, which is of minor importance, especially for the relative measurements described here. Nevertheless, having a magnitude of $A_0$ (which is comparable to $|s_{22}|$ and $|s_{62}|$), the introduced magnitude and phase measurement errors can be estimated using the analysis shown in [20]. Since the magnitude of $A_0$ can be assumed to be $\approx -25$ dB for the used six-port reflectometers, the magnitude

and phase measurement error can be approximated as

$$\Delta_{\text{mag}} \approx 0.11 \cdot |\Gamma| \tag{63}$$
$$\Delta_{\text{phase}} \approx 6.5 \cdot |\Gamma| \, [°] \tag{64}$$

meaning that the maximum error is obtainable for the unitary magnitude of the measured reflection coefficient. By combining (63) and (64), the maximum EVM can be calculated. For $|\Gamma| = 1$, it is equal to 0.162, which fully corresponds to the worst case observed in Fig. 10. Also, for smaller magnitudes $|\Gamma|$, this value becomes proportionally smaller, which is also seen in Fig. 10. It should also be emphasized that such systematic error is of lower importance for measurements normalized to unknown calibration load as in the proposed calibration procedure. For example, the magnitudes measured by the classic six-port reflectometer over the range 2.6–2.8 GHz seen in Fig. 8(a) are uniformly decreased. Hence, the ratio (or difference in dB scale) between any two measurements remains almost unaffected, which is crucial for such normalized measurements.

## VI. CONCLUSION

In this article, a new method for calibrating six-port reflectometers was proposed. It is the first fully analytical calibration procedure, which uses a matched load and unknown calibration loads, which may differ in both magnitude and phase. Since the used calibration loads do not have to share equal magnitudes, arbitrary loads can be used; therefore, requirements on calibration loads are significantly relaxed. To obtain good performance, the corresponding reflection coefficients should, however, be reasonably spread over the complex plane. The procedure requires at least nine different calibration standards, and this number can be arbitrarily increased for higher robustness. Because of the provided closed-form

solution, the proposed method does not require any sophisticated iterative numerical algorithm. Thus, the execution time is greatly reduced with the previously numerical approach reported in [20]. Since it allows for relative measurements of complex reflection coefficients, it may be applied in, e.g., microwave sensors, where phase shift and/or magnitude ratio is subject to measure. Also, it is suitable for implementation in mobile microwave measurement systems having limited computational resources.

The proposed method was experimentally validated using two wideband six-port reflectometers exhibiting different parameters for a wide range of both magnitude and phase of the measured reflection coefficients. The developed calibration procedure ensures high robustness to imperfect power measurement realized with the aid of integrated power detectors. For further inspection, a reference calibration procedure was developed, in which the same calibration loads were used as known values, as their reflection coefficients were previously measured using VNA. The comparison showed that the proposed calibration provides accurate results, being very close to the ones obtained in the reference calibration using known calibration loads and to the reflection coefficients measured using commercial VNA. It is therefore seen that the presented procedure is particularly useful for systems in which the measurement circuitry is integrated with DUT with no possibility to precisely characterize calibration loads, and at most, coarse information regarding their reflection coefficient (e.g., simulation results) is given [25]. Furthermore, it can be seen that the model (1) used in the proposed calibration for one-port measurements is also valid for transmission (two-port) measurements, as discussed in [25]. Hence, future works will be focused on the augmentation of the developed procedure on two-port measurements.

## References

[1] G. F. Engen, "A (historical) review of the six-port measurement technique," *IEEE Trans. Microw. Theory Techn.*, vol. 45, no. 12, pp. 2414–2417, Dec. 1997.

[2] S. O. Tatu, A. Serban, M. Helaoui, and A. Koelpin, "Multiport technology: The new rise of an old concept," *IEEE Microw. Mag.*, vol. 15, no. 7, pp. S34–S44, Nov. 2014.

[3] A. Koelpin, G. Vinci, B. Laemmle, D. Kissinger, and R. Weigel, "The six-port in modern society," *IEEE Microw. Mag.*, vol. 11, no. 7, pp. 35–43, Dec. 2010.

[4] K. Kim, N. Kim, S. Hwang, Y. Kim, and Y. Kwon, "A miniaturized broadband multi-state reflectometer integrated on a silicon MEMS probe for complex permittivity measurement of biological material," *IEEE Trans. Microw. Theory Techn.*, vol. 61, no. 5, pp. 2205–2214, May 2013.

[5] A. O. Olopade, A. Hasan, and M. Helaoui, "Concurrent dual-band six-port receiver for multi-standard and software defined radio applications," *IEEE Trans. Microw. Theory Techn.*, vol. 61, no. 12, pp. 4252–4261, Dec. 2013.

[6] B. Laemmle, G. Vinci, L. Maurer, R. Weigel, and A. Koelpin, "A 77-GHz SiGe integrated six-port receiver front-end for angle-of-arrival detection," *IEEE J. Solid-State Circuits*, vol. 47, no. 9, pp. 1966–1973, Sep. 2012.

[7] V. Adler and K. Hoffmann, "Six-port spatial electromagnetic wave measurement," *IEEE Trans. Microw. Theory Techn.*, vol. 62, no. 12, pp. 3161–3171, Dec. 2014.

[8] K. Haddadi and T. Lasri, "Forward V-band vector network analyzer based on a modified six-port technique," in *Proc. IEEE Topical Conf. Wireless Sensors Sensor Netw. (WiSNet)*, San Diego, CA, USA, Jan. 2015, pp. 23–25.

[9] R. Halir et al., "Integrated optical six-port reflectometer in silicon on insulator," *J. Lightw. Technol.*, vol. 27, no. 23, pp. 5405–5409, Dec. 2009.

[10] I. Molina-Fernández et al., "Multi-port technology for microwave and optical communications," in *IEEE MTT-S Int. Microw. Symp. Dig.*, Montreal, QC, Canada, Jun. 2012, pp. 1–3.

[11] S. Li and R. G. Bosisio, "Calibration of multiport reflectometers by means of four open/short circuits," *IEEE Trans. Microw. Theory Techn.*, vol. MTT-30, no. 7, pp. 1085–1090, Jul. 1982.

[12] J. D. Hunter and P. I. Somlo, "An explicit six-port calibration method using five standards," *IEEE Trans. Microw. Theory Techn.*, vol. MTT-33, no. 1, pp. 69–72, Jan. 1985.

[13] K. Haddadi and T. Lasri, "Formulation for complete and accurate calibration of six-port reflectometer," *IEEE Trans. Microw. Theory Techn.*, vol. 60, no. 3, pp. 574–581, Mar. 2012.

[14] F. Wiedmann, B. Huyart, E. Bergeault, and L. Jallet, "A new robust method for six-port reflectometer calibration," *IEEE Trans. Instrum. Meas.*, vol. 48, no. 5, pp. 927–931, Oct. 1999.

[15] K. Staszek, P. Kaminski, A. Rydosz, S. Gruszczynski, and K. Wincza, "A least-squares approach to the calibration of multiport reflectometers," in *Proc. IEEE MTT-S Int. Microw. RF Conf.*, Delhi, India, Dec. 2013, pp. 1–4.

[16] T. Yakabe, M. Kinoshita, and H. Yabe, "Complete calibration of a six-port reflectometer with one sliding load and one short," *IEEE Trans. Microw. Theory Techn.*, vol. 42, no. 11, pp. 2035–2039, Nov. 1994.

[17] D. Hui and R. M. Weikle, "Calibration of six-port reflectometers using null double injection," in *Proc. 67th ARFTG Conf.*, San Francisco, CA, USA, Jun. 2006, pp. 164–179.

[18] S. Linz et al., "I/Q imbalance compensation for six-port interferometers in radar applications," in *Proc. 44th Eur. Microw. Conf.*, Rome, Italy, Oct. 2014, pp. 746–749.

[19] C. Will et al., "Segmental polynomial approximation based phase error correction for precise near field displacement measurements using six-port microwave interferometers," in *Proc. IEEE Topical Conf. Wireless Sensors Sensor Netw. (WiSNet)*, Phoenix, AZ, USA, Jan. 2017, pp. 23–25.

[20] K. Staszek, "Six-port calibration utilizing matched load and unknown calibration loads," *IEEE Trans. Microw. Theory Techn.*, vol. 66, no. 10, pp. 4617–4626, Oct. 2018.

[21] G. F. Engen, "Calibrating the six-port reflectometer by means of sliding terminations," *IEEE Trans. Microw. Theory Techn.*, vol. MTT-26, no. 12, pp. 951–957, Dec. 1978.

[22] K. Staszek, S. Gruszczynski, and K. Wincza, "Design and accuracy analysis of a broadband six-port reflectometer utilizing coupled-line directional couplers," *Microw. Opt. Technol. Lett.*, vol. 55, no. 7, pp. 1485–1490, Jul. 2013.

[23] K. Staszek, S. Gruszczynski, and K. Wincza, "Six-port reflectometer providing enhanced power distribution," *IEEE Trans. Microw. Theory Techn.*, vol. 64, no. 3, pp. 939–951, Mar. 2016.

[24] K. Staszek, "Six-port reflectometer insensitive to power detectors' impedance mismatch," *IEEE Access*, vol. 10, pp. 89072–89082, 2022.

[25] R. Smolarz, K. Staszek, K. Wincza, and S. Gruszczynski, "A 24 GHz microwave sensor with built-in calibration capability designed in MMIC technology," *IEEE Access*, vol. 9, pp. 31513–31524, 2021.

**Kamil Staszek** received the M.Sc., Ph.D., and D.Sc. (habilitation) degrees in electronics engineering from the AGH University of Science and Technology, Kraków, Poland, in 2011, 2015, and 2019, respectively.

He is an Associate Professor with the Department of Electronics, AGH University of Science and Technology. He has more than two years of industrial experience in automotive radars development. He has coauthored over 90 journal and conference scientific papers. His main scientific interests are multiport measurement techniques in sensor applications and the design of broadband passive components.

Dr. Staszek has been a member of the Technical Program Committee of the International Conference on Microwaves, Radar, and Wireless Communications (MIKON) since 2016. From 2019 to 2023, he was the Junior Vice-Chair of the Polish Section of the International Union of Radio Science (URSI)—Commission A.